

Sandwich-like polythioetherimide-decorated polypropylene (Celgard2400) composite separators with heat resistance and wettability for safety lithium-ion batteries

Haoran Xu¹, Kai Han¹, Meng Li¹, Wen Li¹, Xiaoqi Chen², Jijun Xiao^{1,*}, Yantao Li^{2,*}

¹ School of Materials Science and Engineering, Hebei Engineering Laboratory of Aviation Lightweight Composite Materials and Processing Technology, Hebei Key Laboratory of Material Near-Net Forming Technology, Hebei University of Science and Technology, Shijiazhuang, 050018, People's Republic of China

² Institute of Energy Source, Hebei Academy of Sciences, Shijiazhuang, 050081, People's Republic of China

*E-mail: jijunxiao@aliyun.com, 13903116163@163.com

Received: 9 September 2019 / Accepted: 30 October 2019 / Published: 30 November 2019

We describe a sandwich-like composite separator with two sheath layers of polythioetherimide (PTEI) and a core layer of Celgard2400 to improve the heat-resistance and wettability properties of polypropylene (Celgard2400) separators for lithium-ion batteries (LIBs). The porous PTEI membranes were prepared by a wet phase inversion process and coating with Celgard2400 via engaging a simple process without adhesive. The separators were characterized by thermogravimetric analysis, scanning electron microscopy, and contact angle measurements, and the electrochemical performances were evaluated. The results showed that the PTEI/Celgard2400/PTEI composite separators exhibited excellent thermal stabilities (-37% at 180°C), improved wettabilities, liquid electrolyte uptakes (298%) and ionic conductivities (0.59 mS cm^{-1}) relative to Celgard2400. Compared to the Celgard2400 separator cell, the PTEI/Celgard2400/PTEI composite separators exhibited almost identical electrochemical properties. Such composite separators with high heat-resistance and wettability properties have a great potential for applications in high-safety LIBs.

Keywords: Polythioetherimide; Heat resistance; Composite separator; Electrochemical performance; Lithium-ion battery

1. INTRODUCTION

In recent years, lithium-ion batteries (LIBs) with excellent cycle lives and power densities have become an increasingly promising power source in new large-scale applications. They have enabled

extensive applications, from consumer electronics to transportation [1, 2]. LIBs must be safe, affordable, and low maintenance with high-energy densities and power capacities. However, most recent research into LIB components has focused on electrochemically active materials, such as cathodes, anodes, and electrolytes, to achieve higher energy densities; however, the safety of the separators has been rarely examined [3-5].

The separator is a key component of the liquid electrolyte LIB. It is sandwiched between the cathode and anode to prevent the physical contact of the electrodes [6]. Common commercial separators for LIBs use polyolefin materials [7, 8]. Under abnormal circumstances, such as overcharging and physical crushing, LIBs can generate a large amount of heat and melt the separator, resulting in a potentially dangerous short circuit due to immediate contact between the cathode and anode. In addition, the polyolefin separator has a poor surface wettability in the electrolyte; thus, further LIB developments will also be affected by the performance of the polyolefin separators [9].

There have been many attempts to create separators with higher thermal stabilities. The main methods are the application of cross-linked polymers [10, 11], thermal resistance polymers [12-14], or ceramic nanoparticles [5,15-18] as coatings. Chung used cross-linked polymers containing diethylene glycol dimethacrylate (DEGDMA), and the shutdown and meltdown temperatures of these separators increased to 142°C and 155°C, respectively [10]. Kong prepared polyetherimide (PEI) fibrous separators using an *in situ* micro-melting technique and electrospinning[19]. The separator did not shrink below 240°C, and the cell with this separator had a higher capacity (113.3 mAh·g⁻¹, 5C) than that with a Celgard2400 separator (95.2 mAh·g⁻¹, 5C). Lee introduced copolyimide (PI) as a polymer binder and an Al₂O₃/polymer composite surface coating on a polypropylene (PP) separator to improve the thermal stability of the separator, and the Al₂O₃/PI-coated PP separators efficiently impeded the thermal shrinkage (-10% at 150°C) [5]. These thermally resistant separators could retain dimensional stability and effectively isolate the electrodes to prevent the cell from short-circuiting and exploding at high temperatures [20].

PI is widely known as a polymer with a high temperature resistance, remarkable mechanical strength, good chemical resistance, and a low dielectric constant [21]. It has been widely used in many fields [22, 23]. At present, formation methods for the PI separator used in LIBs mainly include electrostatic spinning and phase separation processing. PI exhibits good thermal stability and dimensional stability at high temperatures [12, 24]. However, the excessively large pore size and broad pore size distribution of these PI nonwoven separators usually lead to severe liquid electrolyte leakage and self-discharge, which deteriorates the cell safety and electrochemical performance and finally hinders their successful application in LIBs [20,25]. The solvents used in the phase separation process damage the thermal stability and mechanical properties to some extent. In addition, while these polyimide separators have high thermal stabilities, they do not have relatively low closed-cell temperatures. A common method to reduce the obturator temperature is to coat the surface of the polymer with lower melting point materials [26, 27].Although PP/PE/PP separators have been commercially produced, the product is still very limited due to the nature of the polyolefin separators [27]. Studies on sandwich structures (PI/PP/PI) for LIB applications are relatively rare but could have value. In this study, a soluble PI porous membrane was introduced on both sides of a PP separator via a phase separation method.

In our work, a series of polythioetherimide (PTEI)/Celgard2400/PTEI composite separators for LIBs were fabricated in which polyamic acid was synthesized from 3,3'-dimethyl-4,4'-diaminodiphenylmethane (MDT) and three isomeric diphenylthioether dianhydrides (m-TDPA) via polycondensation. The material was then chemically imidized at room temperature. PETI membranes with different porosities were prepared via phase separation. The effects of porosity on the thermal shrinkage, electrolyte wettability, and ionic conductivity properties of PTEI/Celgard2400/PTEI composite separators were investigated. Furthermore, the electrochemical performances of cells assembled with PTEI/Celgard2400/PTEI composite separators were demonstrated and compared with those of cells assembled with Celgard2400 separators.

2. EXPERIMENTAL

2.1. Materials

The MDT was provided by the Sinopharm Chemical Reagent Co., Ltd., China. Three isomeric diphenylthioether dianhydrides (m-TDPA) were provided by Ningbo Institute of Materials, Chinese Academy of Sciences. Methanol, N,N-dimethylformamide (DMF), N-butanol, N,N-dimethylacetamide (DMAC), triethylamine, and anhydrous ethanol were provided from Shanghai Aladdin Bio-Chem Technology Co., Ltd. The liquid electrolyte (1 M LiPF₆, ethylene carbonate (EC)/dimethyl carbonate (DMC)/ethyl methyl carbonate (EMC) in a 1:1:1 ratio by weight) was supplied by Guotai Huarong Company, China. Commercially available Celgard2400 was used, which was 20 μm thick.

2.2. Synthesis of PTEI

The synthesis of PTEI (Fig. 1) used 4 g (8.84 mmol) of MDT and 30 ml of DMF placed in a 50-ml three-necked flask under a nitrogen atmosphere with mechanical stirring. After the MDT was completely dissolved, 2.8844 g (8.84 mmol) of m-TDPA was mixed in batches for 0.5 h and stirred at room temperature for 24 h to obtain a viscous polyamic acid solution. Next, 6 ml of acetic anhydride and 2 ml of triethylamine were added to the polyamic acid, stirred at room temperature for 24 h, and poured into 500 ml of methanol. The precipitate solid was filtered and extracted with methanol in a Soxhlet extractor for 6 h. This was then dried under a vacuum at 80°C overnight, resulting in a light grey powder of PTEI.

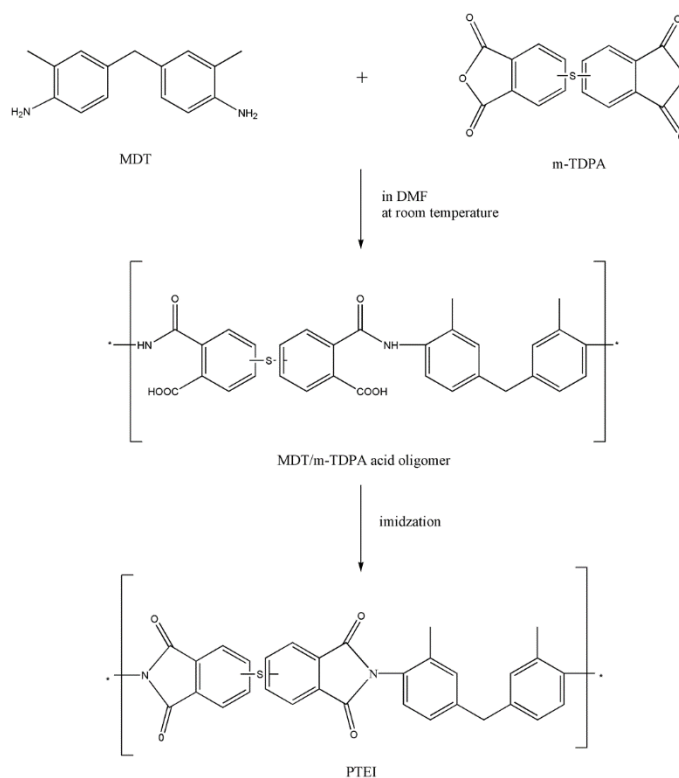


Figure 1. Synthesis of PTEI

2.3. Preparation of the PTEI/Celgard2400/PTEI composite separator

Based on Wang's method, a series of porous PTEI membranes were prepared by phase separation from the PTEI solution using the following procedure [24]. First, PTEI was added to DMAC and stirred until completely dissolved, followed by filtration with an arenaceous filter and degassing. The PTEI solution was subsequently poured on a glass plate and scraped into a film with an applicator. It was then immediately immersed in a non-solvent condensation bath (distilled water: DMAC = 1:1 volume ratio) and held for 5 min to form a porous PTEI membrane.

Five minutes later, the Celgard2400 membrane was covered with a PTEI membrane on all sides. Filter paper was used to absorb excess solution on the membrane, after which the membrane was vacuum dried at 40°C for 8 h to obtain PTEI/Celgard2400/PTEI composite separators. The PTEI/Celgard2400/PTEI composite separators were prepared with concentrations of PTEI solutions of 10, 15, and 20 wt%, which were named CS-1, CS-2, and CS-3, respectively.

2.4. Characterization

The chemical constituents of the PTEI were characterized by attenuated total reflectance Fourier-transform infrared spectroscopy (FTIR/ATR) (S5, Nicolet, US). The microstructures of the separators were observed by scanning electron microscopy (SEM) (S-4800-I, Hitachi, Japan). The electrolyte wettabilities of the separators were determined using two different methods: electrolyte drop and contact angle tests. The contact angles on the separators were measured using an optical

contact angle measuring instrument (DSA100, KRÜSS, German), and the electrolyte drop test was conducted by comparing the electrolyte wetting areas of the Celgard2400 and composite separators. In the electrolyte uptake test, the dried separators were completely immersed in the electrolyte for 4 h in the glove box, and excess electrolyte on the surface was removed. The liquid electrolyte uptake was calculated via the following formula: electrolyte uptake = $(W_1 - W_0)/W_0 \times 100\%$, where W_0 and W_1 are the weights of the membrane before and after immersion, respectively [23].

The porosity values (ε) of the porous membranes were determined by the n-butanol soaking method, in which the weights of the membranes were measured before and after soaking in n-butanol for 2 h at room temperature and calculated using the following equation [28]: $\varepsilon = (W_a - W_b)/(\rho_L \times V_0)$, where W_a is the weight of the n-butanol soaked separator, W_b is weight of the dry separator, ρ_L is the density of n-butanol, and V_0 is the geometric volume of the separator. The thermal stability was examined using a thermogravimetric analyzer (TGA) (TA Instruments, USA, TA Q50) at a heating rate of 20°C/min under dry flow of N₂. The size stabilities of the separators were measured at 165°C and 180°C for 0.5 h.

The ionic conductivity of the separator was obtained as follows: $s = L/(R_b \cdot S)$, where R_b , L , and S are the bulk impedance (ohm), thickness (cm), and effective area (cm²), respectively. Stainless steel plates were used as positive and negative electrode materials. The separator was placed between two metal plates and assembled into an SS/separator–liquid electrolyte/SS system. The spectra were recorded from 0.1 to 10⁵ Hz with an AC amplitude of 10 mV at room temperature on an electrochemical station (Gamry, USA). The interfacial resistance (R_{int}) was measured using a similar method to that for R_b using the Li/separator–liquid electrolyte/Li assembly.

In an Ar glove box, the separator was placed between the positive LiCoO₂ and the negative Li electrodes to assemble a C2032 battery. The initial charge–discharge capacities and cycle performances of the coin cells were investigated using a battery tester (CT2001A, LANHE System, China) within a voltage range of 3.0–4.4 V at 0.5C. The rate capability tests were performed at current densities of 0.5, 1, 2, 3, 4, and 5C in within a voltage range of 3–4.4 V.

3. RESULTS AND DISCUSSION

3.1. FTIR and TGA of separators

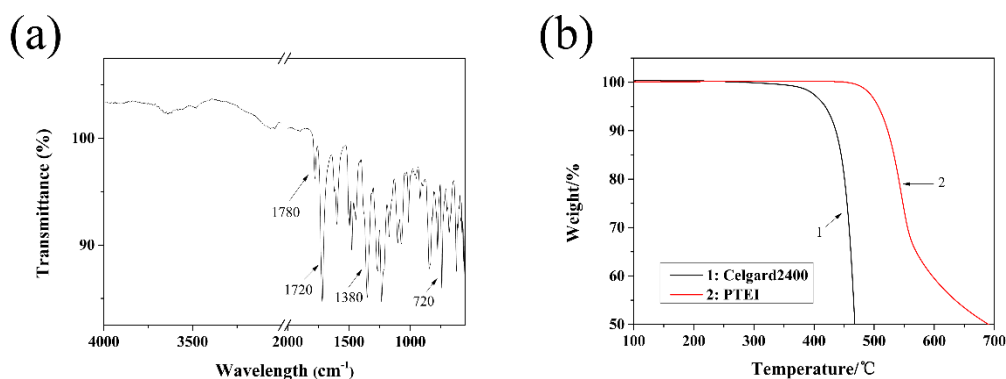


Figure 2. (a) FTIR spectrum of PTEI. (b) TGA of PTEI and Celgard2400 separator.

The chemical structure of the PTEI was analyzed using ATR-FTIR (Fig. 2(a)). The characteristic absorption peaks of polyimide were observed near 725 cm^{-1} (C=O, asymmetric bending vibrations), 1380 cm^{-1} (C–N, asymmetric stretching vibrations), 1720 cm^{-1} (C–O, symmetric stretching vibrations), and 1780 cm^{-1} (C–O, asymmetric stretching vibrations). The characteristic N–H stretching vibrations of the amino groups in polyamic acid in the $3300\text{--}3500\text{ cm}^{-1}$ range were not observed in the ATR-FTIR spectrum, implying that the polymer was fully imidized [24]. The TGA curves (Fig. 2(b)) revealed that the temperatures at which 5% weight loss occurred for the PTEI and Celgard2400 were 506 and 418°C , respectively. Moreover, the temperatures at which 50% of the sample weight remained were 690 and 467°C , indicating that the PTEI separator had a better thermal stability than the Celgard2400 separator. This may have been because the PI separator contained incorporated aromatic rings on the backbone and/or side groups [23]

3.2. Surface morphologies of separators

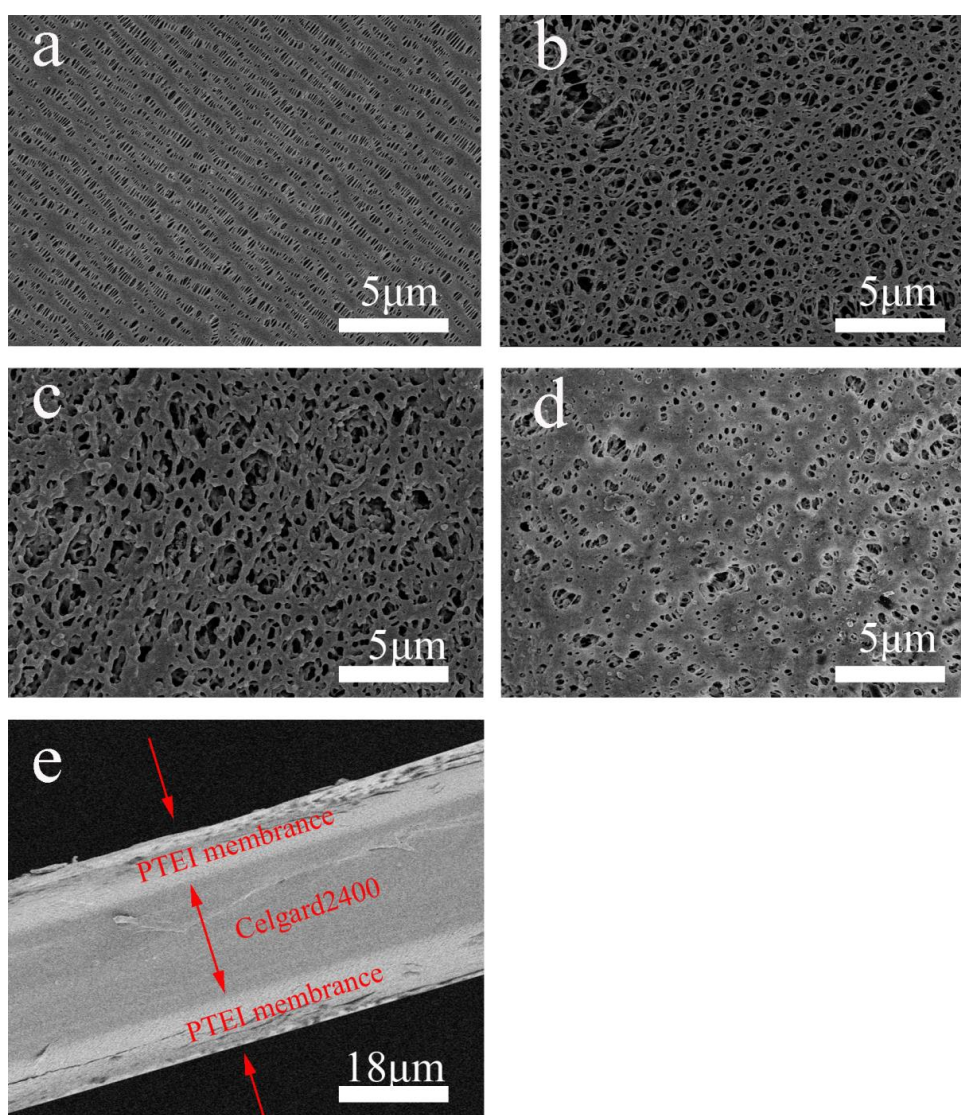


Figure 3. Surface morphologies of (a)Celgard2400, (b)CS-1, (c)CS-2, (d)CS-3 and (e)cross-section

The surface microstructures of the Celgard2400 and PTEI composite separators, as well as a cross-section of the PTEI/Celgard2400/PTEI composite separators, are displayed in Fig. 3. Figure 3(a) shows that the Celgard2400 had interconnected submicron pores. These pores facilitated the transport of lithium ions through the separator and the block the transfer of electrons. The surface morphologies of the PTEI separators are shown in Fig. 3(b)–(d). Compared with the Celgard2400 separator, all of the surface morphologies of PTEI showed larger microporous structures that could absorb more electrolytes and allow lithium ions to be transported. The porous structure of the separator was affected by the phase inversion rate, which was mainly controlled by the diffusion rate of the solvent and non-solvent [22,24]. The PTEI separators prepared by the PTEI solution with different concentrations and the same coagulation bath had different porous structures. This indicated that a higher concentration of PTEI solution led to a stronger ability to hinder non-solvent diffusion. Therefore, the porosity of the PTEI separator decreased with increasing concentration of the PTEI solution. Figure 3(e) shows the cross-section of the PTEI/Celgard2400/PTEI composite separators. The thicknesses of the PTEI and Celgard2400 were approximately 20 and 20 μm , respectively. Although no adhesive was used, the PTEI and Celgard2400 separator was strongly bonded at their interface, indicating that PTEI had adhesion with the Celgard2400.

3.3. Thermal stability of separator

If the separator is destroyed, the LIBs can have a thermal event or even combust or explode. Therefore, it is very important for the separator to have size stability at high temperatures. The thermal stabilities of the PTEI/Celgard2400/PTEI composite separators and Celgard2400 separator were evaluated by measuring the area changes after heating the separator at 165 and 180°C for 30 min, respectively. Figure 4 shows that shape changes of these separators occurred after thermal treatment, especially in the machine direction (MD) [29] where the separator had been stretched. The Celgard2400 separator exhibited 43% shrinkage in the MD after heat treatment at 165°C for 30 min. The color of the Celgard2400 separator changed from white to semi-transparent. Celgard2400 showed significant shrinkage and was destroyed when heated at 180°C for 30 min, indicating that 180°C was beyond the melting point of the Celgard2400. In contrast, the amounts of thermal shrinkage of CS-1, CS-2, and CS-3 after thermal treatment at 165°C for 30 min were 16%, 15%, and 10%, respectively, and the samples retained their white color. After thermal treatment at 180°C for 30 min, the shrinkage ratios of the CS-1, CS-2, and CS-3 were 37%, 33.3%, and 21%, respectively. This indicated that the PTEI coating was very effective at suppressing thermal shrinkage. This was because PTEI is a polymer with a high thermal stability, and the PTEI coatings were strong enough to withstand the mechanical stress created by the dimensional changes during shrinkage [5]. These results showed that the PTEI/Celgard2400/PTEI composite separator had better thermal stability than Celgard2400 and exhibited a higher thermal safety performance.

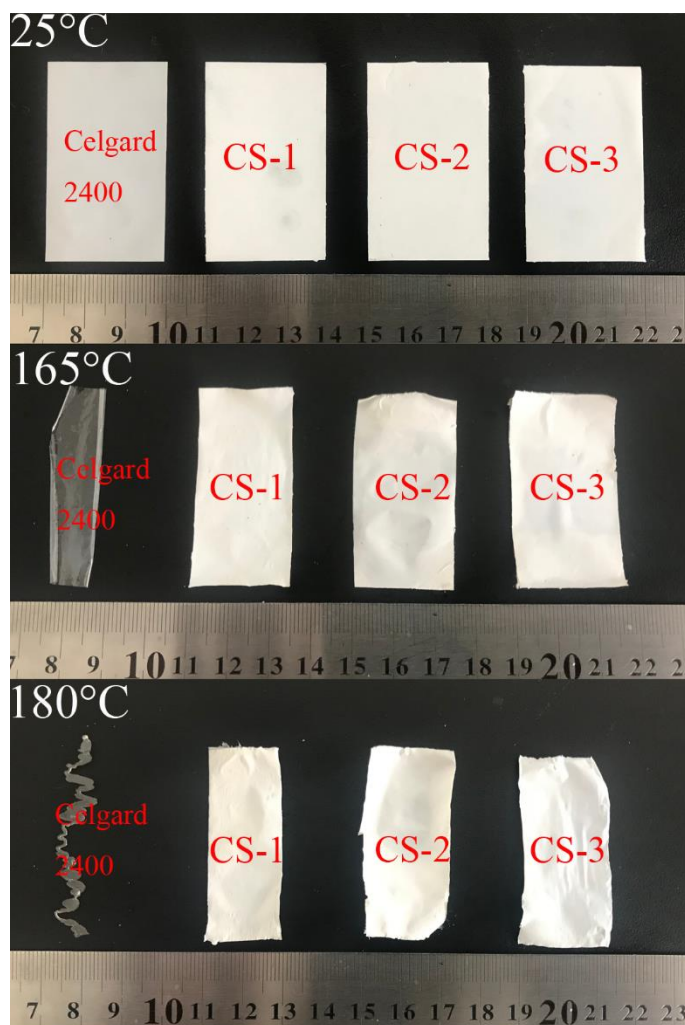


Figure 4. Real shape change of the Celgard2400 and CS-1, CS-2 and CS-3 at different temperatures.

Previous studies mainly used separators with high thermal stabilities or nanoporous particle-coated polyolefin separators [13-19]. Separators that were prepared by thermally stabilizing polymers, although having outstanding thermal stabilities, lacked a low closed-cell temperature, thereby failing to effectively improve LIB safety [26,27]. Furthermore, achieving ideal results using ceramic nanoparticle-modified membranes is difficult due to uneven coating and nanoparticles detaching from the membranes. The separator prepared in this paper not only improved the thermal stability of Celgard2400, but it also retained the low closed-cell temperature of Celgard2400, which is very important for lithium ion batteries.

3.4. Wettability of separator

The wettability of a separator is very important for investigating the performances of LIBs [24], and a separator should absorb and hold a significant amount of liquid electrolyte [30-32]. The wettability properties of the separators prepared in this study were measured by measuring the contact

angles of the electrolyte on the separators (Fig. 5). The contact angles on the Celgard2400, CS-1, CS-2, and CS-3 were 45.3° , 10° , 12.4° , and 18.6° , respectively. The PTEI/Celgard2400/PTEI composite separators had better wettabilities than that of Celgard2400, which has a low surface energy and is naturally hydrophobic [30, 31, 33]. However, the surfaces of the PTEI/Celgard2400/PTEI composite separator were PTEI membranes, which had higher surface polarities due to the polar nature of the imide structure, which allowed it to exhibit better wettability in the liquid electrolyte [34]. Moreover, the differences in the pore structure, surface roughness, and hydrophobicity of the PTEI/Celgard2400/PTEI composite separator also resulted in different contact angles. Figure 6 shows that the liquid electrolyte dropped on the Celgard2400 separator was not absorbed, whereas it was easily and quickly absorbed by the composite separators. Such a fast absorption rate can shorten the activation time during the battery assembly process [20].

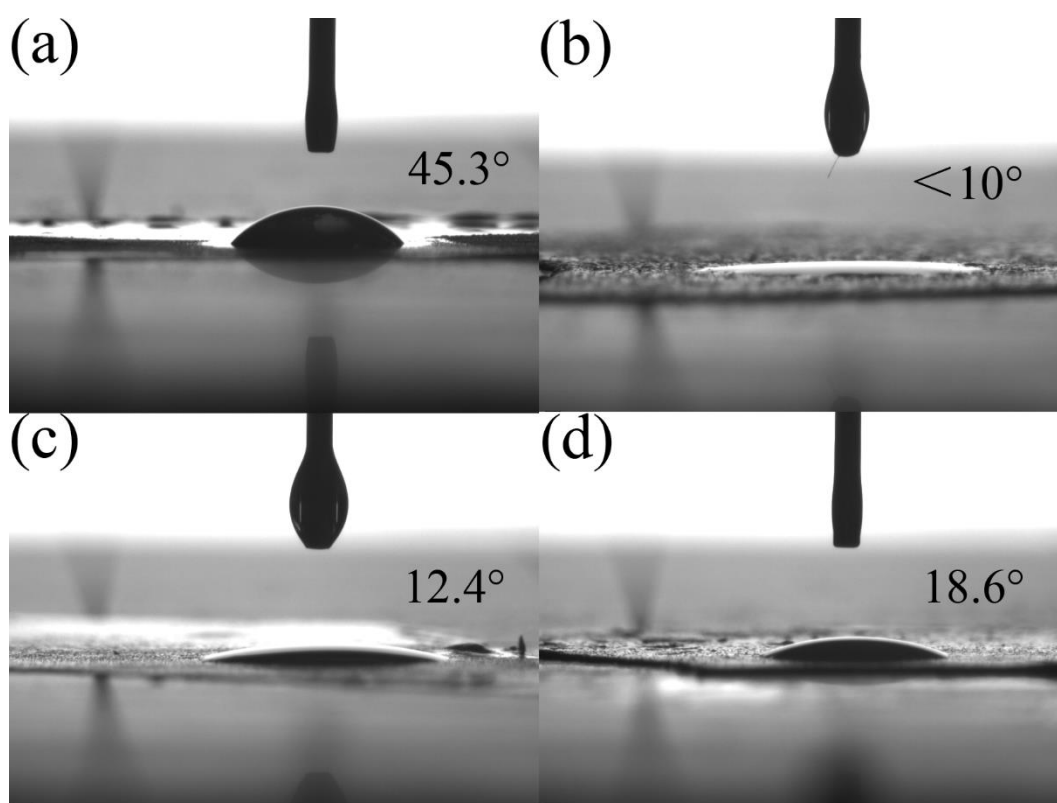


Figure 5. Photographs of contact angle of separator: (a) Celgard2400, (b) CS-1, (c) CS-2, and (d) CS-3.

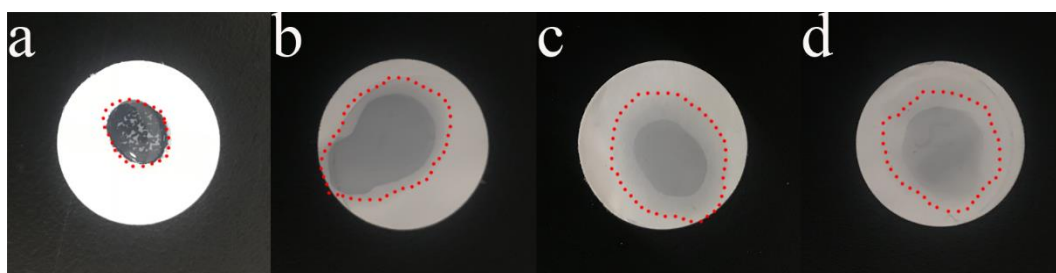


Figure 6. Different separators of liquid electrolyte wettability: (a) Celgard2400, (b) CS-1, (c) CS-2, and (d) CS-3.

3.5. Liquid electrolyte uptake, ionic conductivity, and interfacial impedance

A maximum electrolytic mass in the separator is ideal to achieve minimum internal resistance of the battery [29, 35]. Electrolyte absorption is determined by mass changes in the separators before and after immersion in the liquid electrolyte. The ionic conductivities and liquid electrolyte uptake of the Celgard2400 and PTEI/Celgard2400/PTEI composite separators with PTEI membranes with different porosities were examined, and the results are shown in Table 1. The porosity of the PTEI/Celgard2400/PTEI composite separator decreased from 72% (CS-1) to 47% (CS-2), and the liquid electrolyte uptake of the PTEI/Celgard2400/PTEI composite separator decreased from 298% (CS-1) to 192% (CS-2). These values were higher than that of the Celgard2400 separator, indicating that CS-1 and CS-2 had higher porosities and polarities than the Celgard2400. The uptake then decreased to values less than that of the Celgard2400 separator with a further decrease in the porosity of the PTEI/Celgard2400/PTEI composite separators. This indicated that porosity played a major role in the uptake.

Table 1. Electrolyte uptake, porosity, and ionic conductivity of the separators.

ID	Thickness (μm)	Porosity (%)	Electrolyte uptake (wt%)	Ionic conductivity (mS cm^{-1})
Celgard2400	20	45	183	0.50
CS-1	39	72	298	0.59
CS-2	42	47	192	0.46
CS-3	40	37	176	0.42

Figure 7(a) shows the Nyquist plot and the bulk resistance (R_b) values of the cells for the Celgard2400, CS-1, CS-2, and CS-3 separator samples, as well as the ionic conductivity values of the separators. The bulk resistance values for the Celgard2400, CS-1, CS-2, and CS-3 were 1.56, 2.61, 3.58, and 3.71 Ω , respectively, and their corresponding ionic conductivities (Table 1) were 0.50, 0.59, 0.46, and 0.42 mS cm^{-1} , respectively. The bulk resistance of Celgard2400 (1.56 Ω) was lower than that of CS-1 (2.61 Ω). However, the ionic conductivity of CS-1 reached a maximum value of 0.59 $\text{mS}\cdot\text{cm}^{-1}$, which is higher than that of Celgard2400, indicating that the pores of CS-1 had high electrolyte retention [36, 37] and that the CS-1 had a higher porosity, which would provide rapid mobility for the lithium ions. Therefore, CS-1 was the best composite separator for electrochemical measurements.

The interfacial compatibility of the liquid-electrolyte-soaked separator with a lithium electrode was characterized via electrochemical impedance spectroscopy [12]. Figure 7(b) shows that the cell with CS-1 had a smaller interfacial resistance (R_{int} about 124 Ω) than that with the bare separator (about 200 Ω). This lower interfacial resistance of CS-1 can be explained by its higher liquid electrolyte

uptake [20,38] and higher porosity. PTEI improved the compatibility between the separator and the electrodes to help decrease the capacity loss in practical battery applications [20].

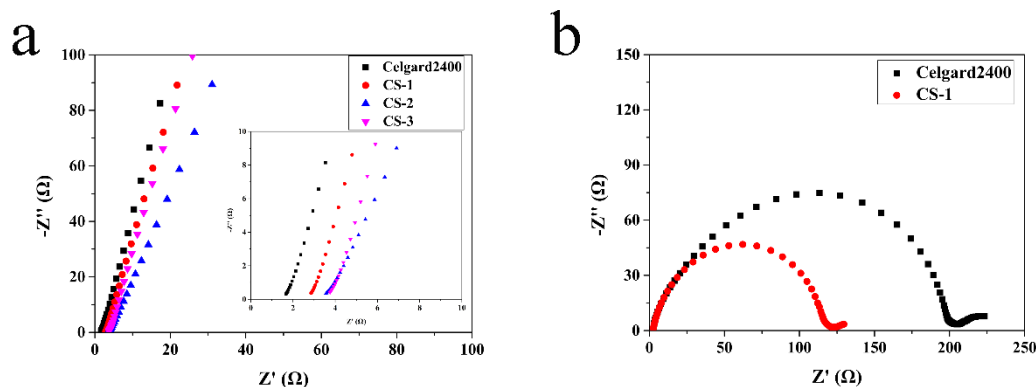


Figure 7. Nyquist plots of (a) Celgard2400, CS-1, CS-2, and CS-3 and (b) Celgard2400 and CS-1..

3.6. Battery performance

The discharge curves at 0.5C for different cycles of the CR2032-type coin cells assembled with Celgard2400 and CS-1 are illustrated in Fig. 8. Both cells exhibited nearly identical potential plateaus. The cell with CS-1 had a slightly larger values of the discharge capacity during the first discharge cycle (158 mAhg⁻¹) and after 100 cycles (144 mAhg⁻¹) than the Celgard2400 cell during the first discharge (155.6 mAhg⁻¹) and after 100 cycles (139 mAhg⁻¹). The capacity retention ratio for the cell with CS-1 was higher than that of the cell with Celgard2400 (Fig. 9). Both cells showed a high coulombic efficiency up to 96% after 100 cycles, indicating that the cell with CS-1 had good cycle performance and benefited from the higher porosity and better absorption of the liquid electrolyte [5].

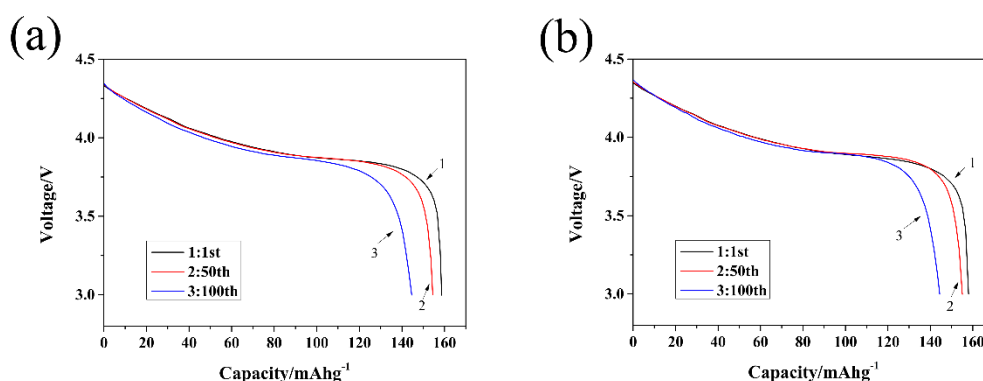


Figure 8. Discharge profiles of (a) Celgard2400 and (b) CS-1

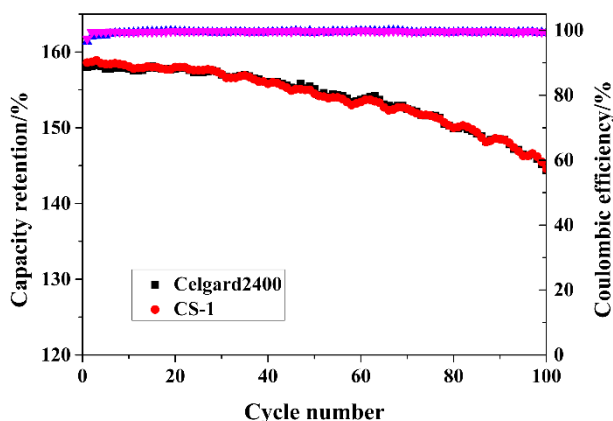


Figure 9. Cycling performance of the cells with Celgard2400 and CS-1 in 100 cycles at current density of 0.5 C.

In addition to the good cycling stability, the rate capability also plays an essential role in LIBs [21]. The charging curves at different rates of 0.5C, 1C, 2C, 3C, 4C, and 5C are shown in Fig. 10. The cell with CS-1 had almost identical charging curves to those of the Celgard2400 separator, and there were no unstable curves observed from 3 to 4.4 V. The results showed that the capacity retention decreased gradually with increasing charge rate, but the capacitance retention ratios were similar (78.2% and 79.4%, respectively). A similar phenomenon can also be observed in Fig. 11. The cells were charged at various rates ranging from 0.5C to 5.0C continuously for five cycles each. The rate capabilities of the Celgard2400 and CS-1 cells were similar. The similar rate capacities were attributed to the sandwich-like structures with large pores in the composite separators. This was due to the porous nature of the coating layer, which did not hinder Li ion diffusion through the separators [39]. This shows that the battery with CS-1 had the same rate capability as the battery assembled with Celgard2400.

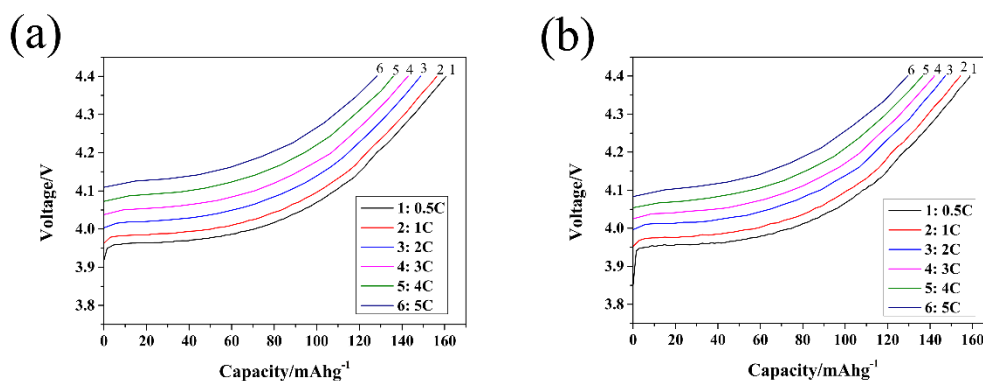


Figure 10. Charge profiles of (a) Celgard2400, (b) CS-1 at different current density from 0.05C to 5C.

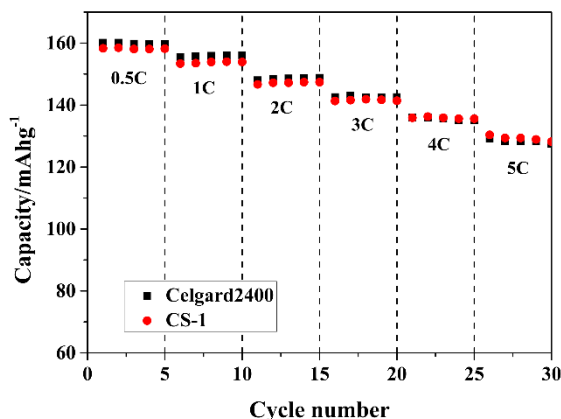


Figure 11. Rate capability of the cells assembled with Celgard2400 and CS-1 separator.

Table 2 shows the results for the traditional polyolefin Celgard2400 separator and several separators with better thermal stabilities. Although Celgard2400 has a high tensile strength, its low porosity and poor thermal stability limit the application of the separator. In this work and in two previous studies [5, 43], composite separators were prepared. Under normal circumstances, the composite separators not only retained good tensile strength, but also the thermal stabilities of the separators improved. Unlike the ceramic nanoparticle composite separators in previous studies [5, 43], the surface pore structure of the composite separator in this work was more uniform, and the nanoparticles did not easily detach. In several studies, separators with more thermally stable polymers were prepared [20, 24, 40, 41, 42]. Although the separators had better thermal stabilities, they lacked a low closed-cell temperature. These separators had relatively low tensile strengths and were more susceptible to damage.

Table 2. Thickness, thermal stability, porosity, tensile strength, and preparation technology

Materials	Preparation technology	Porosity (%)	Thermal stability (%)	Tensile strength (MPa)	References
Celgard2400	/	42	165°C 30 min 43%	124 (MD)	20
CS-1	Coated composite	72	165°C 30 min 16%	/	This work
PI	Phase inversion	61	200°C 30 min < 1%	22.6	24
PI	Phase inversion	72.4	200°C 30 min < 1%	17.5	20
PVDF-HFP	Phase inversion	60	160°C 30 min < 9%	9.63	40
Al ₂ O ₃ /PP	Coated composite	/	165°C 30 min 19%	/	5
PAN	Electrospinning	64	200°C 60 min < 1%	/	41
PEI	Electrospinning	79	No change at 240°C storage	< 21	42
SiO ₂ /PP	Coated composite	50.5	170°C 30min 8.3%	/	43

4. CONCLUSIONS

A series of PTEI/Celgard2400/PTEI composite separators were successfully prepared by covering a porous PTEI membrane on both sides of a Celgard2400 separator. Sample CS-1 had an adequate ionic conductivity (0.59 mS cm^{-1}) and discharge capacity during the initial discharge cycle (158 mAh g^{-1}) and after 100 cycles (144 mAhg^{-1}), and it exhibited a good cycle stability (96%). These values are higher than those of the Celgard2400 separator. CS-1 remarkably improved the thermal shrinkage at elevated temperatures and lowered the liquid electrolyte contact angle. This addressed the issues of thermal stability and wettability associated with Celgard2400. CS-1 not only maintained a proper porous structure but also showed an almost identical electrochemical performance to that of the cells with Celgard2400 without sacrificing its inherently high battery performance. Thus, CS-1 is a promising candidate for high-power and high-safety LIBs.

References

1. B. Scrosati, J. Hassoun and Y.K. Sun, *Energy Environ. Sci.*, 4 (2011) 3287-3295.
2. K. Baris, B. Rangeet, M. Mathieu, S. Vincent, T. Jean-Marie and C.P. Grey, *J. Am. Chem. Soc.*, 131 (2009) 9239-9249.
3. Y. Lee, M.H. Ryou, M. Seo, J.W. Choi and M.L. Yong, *Electrochim. Acta*, 113 (2013) 433-438.
4. J.H. Kim, J.H. Kim, K.H. Choi, H.K. Yu, J.H. Kim, J.S. Lee and S.Y. Lee, *Nano Lett.*, 14 (2014) 4438-4448.
5. Y. Lee, H. Lee, T. Lee, M.H. Ryou and Y.M. Lee, *J. Power Sources*, 294 (2015) 537-544.
6. S.S. Zhang, *J. Power Sources*, 164(2007) 351-364.
7. J.L. Shi, L.F. Fang, H. Li, Z.Y. Liang, B.K. Zhu and L.P. Zhu, *J. Membr. Sci.*, 429 (2013) 355-363.
8. S.S. Zhang, K. Xu, D.L. Foster, M.H. Ervin and T.R. Jow, *J. Power Sources*, 125 (2004) 114-118.
9. Y.S. Jung, A.S. Cavanagh, L. Gedvilas, N.E. Widjonarko, I.D. Scott, S.H. Lee, G.H. Kim, S.M. George and A.C. Dillon, *Adv. Energy Mater.*, 2 (2012) 1022-1027.
10. Y.S. Chung, S.H. Yoo and C.K. Kim, *Ind. Eng. Chem. Res.*, 48 (2009) 4346-4351.
11. L. Wang, N. Deng, L. Fan, L. Wang, G. Wang, W. Kang and B. Cheng, *Mater. Lett.*, 233 (2018) 224-227.
12. Z. Hong, Z. Yin, Z. Yao, A.E. John, L. Yang, W. Li and B. Zhu, *Electrochim. Acta*, 204 (2016) 176-182.
13. W. Jiang, Z. Liu, Q. Kong, J. Yao, C. Zhang, P. Han and G. Cui, *Solid State Ionics*, 232 (2013) 44-48.
14. Y.E. Miao, G.N. Zhu, H.Q. Hou, Y.Y. Xia and T. Liu, *J. Power Sources*, 226 (2013) 82-86.
15. T. Lee, W.K. Kim, Y. Lee, M.H. Ryou and Y.M. Lee, *Macromol. Res.*, 22 (2014) 1190-1195.
16. X. Shen, C. Li, C. Shi, C. Yang, L. Deng, W. Zhang, L. Peng, J. Dai, D. Wu, P. Zhang and J. Zhao, *Appl. Surf. Sci.*, 441 (2018) 165-173.
17. Y. Choi, J.I. Kim, J. Moon, J. Jeong and J.H. Park, *Appl. Surf. Sci.*, 444 (2018) 339-344.
18. D. Li, D. Shi, Z. Yuan, K. Feng, H. Zhang and X. Li, *J. Membr. Sci.*, 542 (2017) 1-7.
19. L. Kong, B. Liu, J. Ding, X. Yan, G. Tian, S. Qi and D. Wu, *J. Membr. Sci.*, 549 (2018) 244-250.
20. H. Zhang, C.E. Lin, M.Y. Zhou, A.E. John and B.K. Zhu, *Electrochim. Acta*, 187 (2016) 125-133.
21. X. Yan, Y. Wang, Y. Tao, C. Hao, Z. Zhao and S. Guan, *Electrochim. Acta*, 216 (2016) 1-7.
22. Y.Y. Lv, J. Wu, L.S. Wan and Z.K. Xu, *J. phys. chem. c*, 112 (2008) 10609-10615.
23. N. Ohta, T. Sogabe and K. Kuroda, *Carbon*, 39 (2001) 1434-1436.
24. H. Wang, T. Wang, S. Yang and F. Lin, *Polymer*, 54 (2013) 6339-6348.

25. J. Shi, H. Hu, Y. Xia, Y. Liu and Z. Liu, *J. Mater. Chem. A*, 2 (2014) 9134-9141.
26. C. Shi, P. Zhang, S. Huang, X. He, P. Yang, D. Wu, D. Sun and J. Zhao, *J. Power Sources*, 298 (2015) 158-165.
27. J. Shi, S. Tao, H. Hu, Y. Xia and Z. Liu, *J. Power Sources*, 271 (2014) 134-142.
28. Y. Li, H. Pu and Y. Wei, *Electrochim. Acta*, 264(2018) 140-149.
29. P. Arora and Z.J. Zhang, *Cheminform*, 35 (2004) 4419-4462.
30. M.L. Yong, J.W. Kim, N.S. Choi, J.A. Lee, W.H. Seol and J.K. Park, *J. Power Sources*, 139 (2005) 235-241.
31. G. Venugopal, J. Moore, J. Howard and S. Pandalwar, *J. Power Sources*, 77 (1999) 34-41.
32. S.Z. Sheng, *J. Power Sources*, 164 (2007) 351-364.
33. O.Oms, G.B. F, Kelder, M. E, Schoonman, Gerrits And Smedinga, *J. Power Sources*, 97 (2001) 598-601.
34. J.L. Shi, L.F. Fang, H. Li, H. Zhang, B.K. Zhu and L.P. Zhu, *J. Membr. Sci.*, 437 (2013) 160-168.
35. X. Huang, *J. Solid State Electrochem.*, 15 (2011) 649-662.
36. CHOI, JaeWon, CHERUVALLY, Gouri, KIM, DulSun, AHN, JouHyeon, KIM and KiWon, *J. Power Sources*, 183 (2008) 441-445.
37. W. Jiang, Z. Liu, Q. Kong, J. Yao, C. Zhang, P. Han and G. Cui, *Solid State Ionics*, 232 (2013) 44-48.
38. M. Yanilmaz, M. Dirican and X. Zhang, *Electrochim. Acta*, 133 (2014) 501-508.
39. J. Song, M.H. Ryou, B. Son, J.N. Lee, D.J. Lee and Y.M. Lee, *Electrochim. Acta*, , 85 (2012) 524-530.
40. M. Xiong , H. Tang, Y. Wang, Y. Lin, M. Sun and Z. Yin, *J. Power Sources*, 241 (2013) 203-211.
41. T.H. Cho, M. Tanaka, H. Onishi, Y. Kondo, T. Nakamura and H. Yamazaki, *J. Power Sources*, 181 (2008) 155-160.
42. L. Kong, B.Liu, J. Ding. X. Yan, G. Tian, S. Qia and D. Wu, *J Membrane Sci*, 549 (2018) 244-250.
43. Z. Zhang, W. Yuan and L. Li, *Particuology*, 37 (2018) 91-98.